In Proceedings of the 14th International Detonation Symposium, Office of Naval Research, pp. 740–749.

Precursor Detonation Wave Development in ANFO due to Aluminum Confinement

Scott I. Jackson, Charles B. Kiyanda, and Mark Short
Shock and Detonation Physics Group
Los Alamos National Laboratory

Abstract. Detonations in explosive mixtures of ammonium-nitrate-fuel-oil (ANFO) confined by aluminum allow for transport of detonation energy ahead of the detonation front due to the aluminum sound speed exceeding the detonation velocity. The net effect of this energy transport on the detonation is unclear. It could enhance the detonation by precompressing the explosive near the wall. Alternatively, it could decrease the explosive performance by crushing porosity required for initiation by shock compression or destroying confinement ahead of the detonation. At present, these phenomena are not well understood. But with slowly detonating, non-ideal high explosive (NIHE) systems becoming increasingly common, proper understanding and prediction of the effects of high-sound-speed confiners on NIHE is desirable. Experiments are discussed that measured the effect of this ANFO detonation energy transported upstream of the front by a 76-mm-inner-diameter aluminum confining tube. Detonation velocity and front shape were recorded as a function of confiner wall thickness and length. Detonation shape profiles are characteristically different from records with weak confinement and displayed small curvature near the confining surface. This variation was attributed to energy transported upstream modifying the interaction between the NIHE and confiner. Average detonation velocities were seen to increase with increasing confiner thickness, while wavefront curvature decreased due to the stiffer, subsonic confinement. Preliminary D_n-κ analysis of the data was performed and required a modified fitting waveform to properly represent the experimental front shapes. It was concluded that the confiner was able to transport energy ahead of the detonation and that this transport has a definite effect on the detonation by modifying its characteristic shape.

Introduction

Accurate prediction of non-ideal high explosive (NIHE) detonation has become a topic of significant interest in recent years. Non-ideal explosives differ from conventional explosives in that they are usually high-porosity, low-density materials where the fuel and oxidizer are not mixed on a molecular level. As a result, NIHEs typically exhibit low detonation velocities. They also have much larger detonation reaction zones that are centimeters in length, rather than the 100's of microns associated with more ideal explosives.

The detonation velocities observed for many NIHEs are typically below the sound speeds of stiff confining materials, including common metals.

Approved for unlimited release: LA-UR-10-03433

In Proceedings of the 14th International Detonation Symposium, Office of Naval Research, pp. 740–749.

This is in contrast to conventional or ideal high explosives (HEs), where the detonation velocity exceeds the sound speed of most confiners. In ideal HE systems with strong confinement, the detonation drives a shock into the inert confiner and no information propagation in the confiner exceeds the detonation velocity. The confiner is only able to influence the detonation by acting on the reaction zone behind the detonation shock and ahead of the sonic surface. Since the confiner is shocked and ideal HEs have small reaction zones, this implies that increasing the confiner thickness above a few reaction zone lengths has no effect on the detonation velocity. For weakly confined systems, a sonic point exists at the HE-inert interface and the inert is unable to influence the detonation reaction zone.

Low-detonation-velocity, stiffly confined systems contain no inert shock when the confiner sound speed exceeds the detonation velocity. This allows the confiner to transport energy from behind the detonation shock upstream to the unreacted explosive. Such energy transmission can potentially enhance or hinder the detonation by modifying the amount of confinement it experiences. In some cases, this "precursor energy" will drive the confiner surface into the NIHE, compressing it. The precompression can densify the NIHE, increasing its detonation velocity,[1] or even igniting it. However, precompression can also crush porosity out of the NIHE, desensitizing it and leading to local detonation failure. The precursor energy can also cause loss of confinement ahead of the detonation due to fracture, which can also result in detonation failure.[2] Finally, the large reaction zone lengths of NIHEs and the subsonic confinement both allow for a much greater dependence of confiner thickness on detonation velocity.[3]

These types of wall-explosive phenomena are not typically present in most conventional HE configurations. Our current level of physical understanding of this interaction prevents accurate modeling of confined NIHE systems. We seek calibration data for the Detonation Shock Dynamics (DSD) code to resolve this limitation. DSD is able to model detonation propagation when supplied with the detonation velocity variation versus detonation surface curvature and the detonation edge angle at the explosive-confiner interface. The velocity-curvature relationship is derived from experimental rate-stick data. For ideal HEs with shocked confiners, the edge angle can be found from shock polar analysis.[4,5] However, since the confiner flow is shockless and subsonic in NIHEs when the confiner sound speed exceeds the detonation velocity, alternate methods must be implemented. Experimental measurements are required for the development of these new techniques.

In this work, we experimentally characterize the interactions between the detonation front, a stiff confiner, and the unreacted explosive. Ammonium-nitrate-fuel-oil (ANFO) was selected as the NIHE and aluminum tubes were used as confiners. Experimentally observed ANFO detonation velocities range from 1.5–4.0 mm/μs depending on the explosive properties, charge size and degree of confinement,[6] while the longitudinal sound speed of aluminum is in excess of 5.0 mm/μs. Parameters include the confiner wall thickness and detonation run length. We measure the detonation wave speed as well as the velocity of the elastic stress wave that is driven in the metal ahead of the detonation. Detonation front profiles are also recorded at the end of the tube. We then discuss the novel wave shapes encountered in these systems due to the HE-confiner interaction and present a preliminary D_n-κ form for the data to guide DSD analysis.

Aluminum-Confined ANFO Rate Sticks

Experiments were performed to obtain the detonation front-shape and velocity data for aluminum-confined ANFO. All tests used ANFO mixtures consisting of 94% ammonium nitrate prills by weight mixed with 6% No. 2 diesel fuel by weight. Porous, industrial-grade ammonium nitrate was used from Dyno Nobel with a typical bulk density of 0.80 g/cc and an average prill diameter ranging from 1.4–2.0 mm. Mixing was accomplished by combining the prills and diesel fuel in a cement mixer and mixing for a minimum of 15 minutes. ANFO was then poured into each tube in 200-g increments. Each incremental fill was hand-tamped to prevent significant clumping or void formation. This methodology was sufficient to achieve an ANFO density of 0.86–0.90 g/cc.

Aluminum tubes were used to confine the ANFO during the front-shape measurements. Each tube

In Proceedings of the 14th International Detonation Symposium, Office of Naval Research, pp. 740–749.

was 76.2 mm in inner diameter (ID) and wall thickness ranged from 6.35–25.4 mm. The tube lengths were 305 or 914 mm (Tab. 1) yielding length-to-diameter ratios of $L/ID = 4$ and 12. All were 6061 alloy and T6 temper, except for the 25.4-mm-thick tubing, which was T6511. The downstream end of each tube was sealed with a 6.35-mm-ID PMMA window with an outer diameter matching that of the tube (Fig. 1). A centerline on the window contained a line of PETN paint backed by 80-μm-thick copper tape (Fig. 2). Arrival of the detonation shock at this location initiated the PETN with a bright flash that was recorded by a streak camera, yielding the front-shape record.

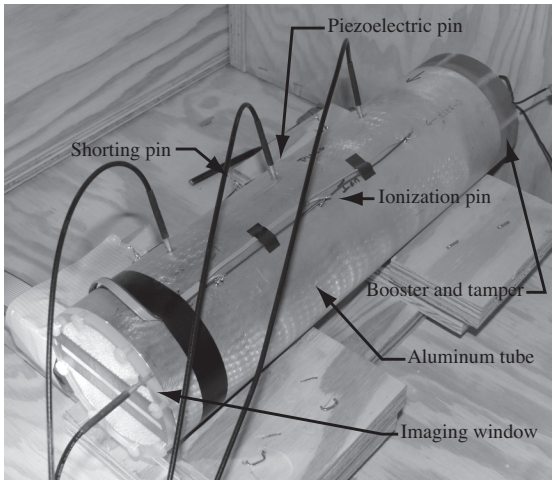

Fig. 1. The tube from test 6-305.

Each aluminum tube also contained three types of diagnostic pins to detect the transit of various waves. These pins were mounted in the wall to be flush with the tube ID. Dynasen ionization (CA-1040) and shorting pins (CA-1038) pins were used to measure the ion and shock arrival, while tightly fitted piezoelectric pins (CA-1136) simultaneously recorded both compression of the tube wall, to detect the precursor stress wave in the aluminum, as well as the arrival of the detonation. Pins were located 83.1-mm axially apart and were spaced 45° deg radially apart (Fig. 3). A piezoelectric pin was also located in the end window against the downstream tube surface. Detonation initiation was accomplished with 12.7-mm-thick Primasheet 1000

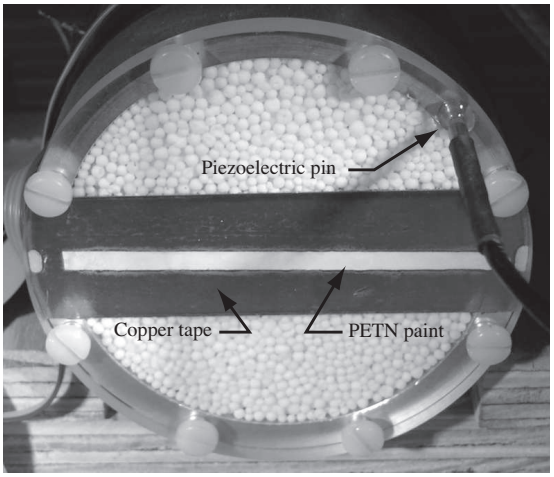

Fig. 2. The downstream end window of the 6.35-mm-thick, 305-mm-long tube filled with ANFO.

booster and an RP-1 detonator, tamped from behind by 12.7-mm of polycarbonate. This booster strength was determined to be sufficient in a separate study.[7] All pins were sampled at 1.25 GHz. The sample rate coupled with the pin spacing provided velocity uncertainties of 1% for the ionization and shorting pins, and 3% for the piezoelectric pins.

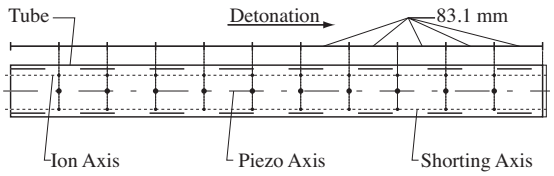

Fig. 3. A schematic of the pin arrangement on the 6.35-mm-thick, 914-mm-long tube.

Pin Velocities and Front-Shape Records

Pin Data

An example of the pin data from test 12-305 is shown in Fig. 4. Early in time, at approximately 24 μs, the arrival of the precursor stress wave is detected by the piezoelectric pin, as denoted by an oscillating waveform of increasing strength. As the detonation front arrives at the pin station near 35 μs, the pin records substantially increased compression, followed by a rapid release that was likely due

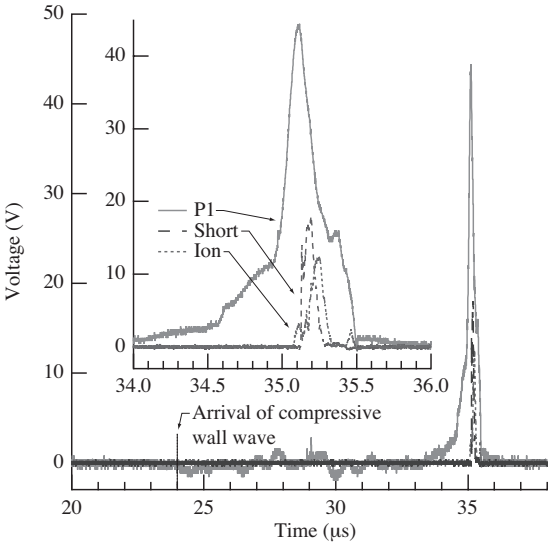

Fig. 4. Example of pin data traces.

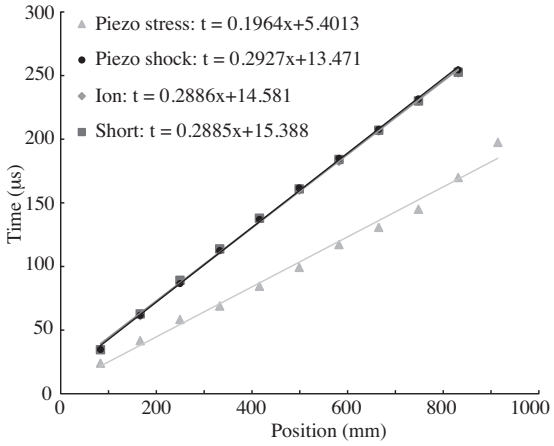

Fig. 5. Position-time diagram for the 12.7-mm-thick, 914-mm-long tube showing pin trigger times and average velocity fits. Ionization, shorting, and piezoelectric shock data are close to being on top of each other.

to pin failure. During the period of increased compression, both the ionization and shorting pins trigger within 100 ns of each other. In every test, all pins at each station triggered within 1 μs of each other. A pin was considered to have triggered when the signal rose above the bit noise associated with the data acquisition system. Additionally, there is a trigger delay inherent in the mechanical design of the shorting pin that requires the shock pressure to move a brass cap across a 64-μm gap, while no such delay exists for either the piezoelectric or ionization pins. This may explain why the shorting pin triggers last.

Pin arrival times from each test were analyzed to yield position-time plots of the wave motion in the experiment. An example of one such plot is shown in Fig. 5 for test 12-914. The progression of the detonation can be seen from the closely matched ionization, shorting and piezoelectric shock pin trigger times. The propagation of the elastic stress wave in the metal is also seen ahead of the detonation front. The data from each pin fit well to a line using a least squares fit, the slope of which yields the average wave velocity in the experiment.

These average wave velocity data are reported in Tab. 1. The velocity of the elastic precursor ranges from 5.1–6.5 mm/μs, which is consistent with the speed of sound in aluminum. Detonation velocities range from 2.7–3.6 mm/μs, increasing with wall thickness up to the maximum 25.4-mm wall thickness tested. As mentioned, this trend was expected due to the extended length of the ANFO reaction zone and the subsonic confinement condition. No inert shocks were present to limit the entire confiner thickness from acting on the reaction zone.[3]

Overall, we find the agreement of the linear velocity fit to the elastic precursor wave data to be good, with squared correlation coefficients above 0.987. The fit to the detonation pin data is excellent, with all squared correlation coefficients above 0.996. The lower fit correlation for the elastic stress wave is attributed to multiple issues: The Primasheet booster overdrives the precursor wall wave initially, as evidenced by the higher elastic wave speeds in the shorter length tubes. Additionally, detection of the elastic precursor signal can be difficult due to its low amplitude, which can be exacerbated by a poorly fit pin not sensing early compression due to insufficient sidewall contact.

The detonation, however, does not exhibit any overdrive associated with the initiation process. In fact, comparison tests of identical wall thicknesses find average velocities that are consistently 3–10% lower for the short tubes, relative to the longer lengths tested, indicating that the wave is slightly

In Proceedings of the 14th International Detonation Symposium, Office of Naval Research, pp. 740–749.

Table 1. Dimensional and average velocity data. Asterisk (*) denotes the T6511 temper tube, all others were T6.

Test Name	Wall Thickess (mm)	Tube Length (mm)	Short Pin Shock U (mm/μs)	Ion Pin Shock U (mm/μs)	Piezo Pin Shock U (mm/μs)	Piezo Stress Wave U (mm/μs)
6-305	6.35	305	2.772	2.690	2.814	5.721
6-914	6.35	914	2.838	2.797	2.904	5.453
12-305	12.70	305	3.125	3.193	3.092	5.615
12-914	12.70	914	3.466	3.465	3.416	5.092
25-305	25.40	305	3.383	3.588	3.377	6.480*

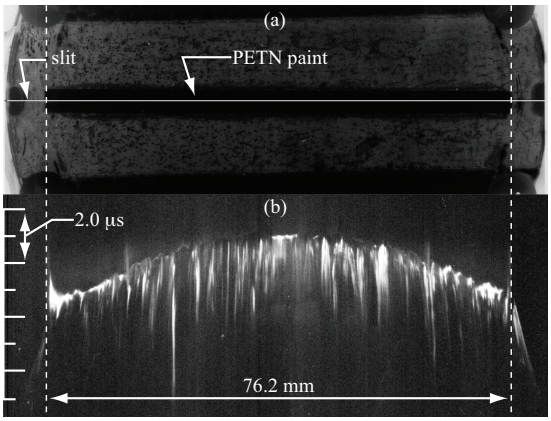

Fig. 6. Still frame (a) and streak image (b) for 6.35-mm-thick, 305-mm-long tube.

underdriven from the booster.

Front-Shape Records: Figure 6 shows the front-shape data for test 6-305. The upper image is a still frame showing the imaging slit of the window in Fig. 2. The lower image is the streak data with time increasing downwards. The granular nature of the explosive is reflected in the streak and some jetting of product gas ahead of the main shock is also evident, particularly at the left wall. Such jetting is also observed in ANFO rate sticks with weaker confinement due to air gaps allowing product gases to rush ahead of the main front. In Fig. 6, the gap is believed to be due to the subsonic wall pulling away from the explosive ahead of the detonation. A more definitive conclusion is not possible in the current study and jetting effects are neglected in the following curvature discussion.

The front-shape profile shows lowest curvature near the tube center, indicating a locally higher propagation velocity in the region most isolated from wall expansion. Curvature increases with increasing radius to a maximum between the tube center and the wall, and then decreases near the wall. Different behavior is observed in more weakly confined systems (Fig. 7), where the detonation curvature is at a minimum at the center and monotonically increases outwards towards the wall. Thus, the aluminum confiner is not only providing additional confinement, but also modifying the characteristic shape of the wavefront.

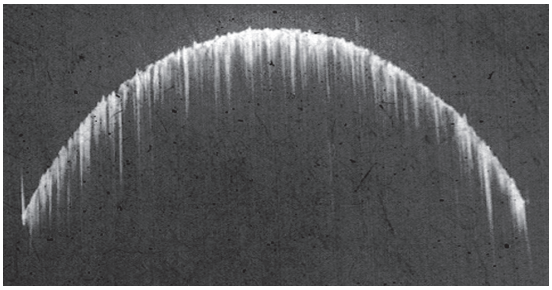

Fig. 7. A streak record from Ref. 6 for ANFO confined by cardboard.

A compilation of all front-shape measurements to date is shown in Fig. 8. All images are identically scaled. Similar features as discussed in Fig. 6 are seen in all traces. It is apparent that increasing the wall thickness not only increases the detonation velocity, but also results in a detonation profile with less overall curvature. Such behavior agrees well with theory.[3] Jetting aside, all fronts also appear fairly symmetric.

Comparison of the leading front in each record shows little difference between the short- and long-

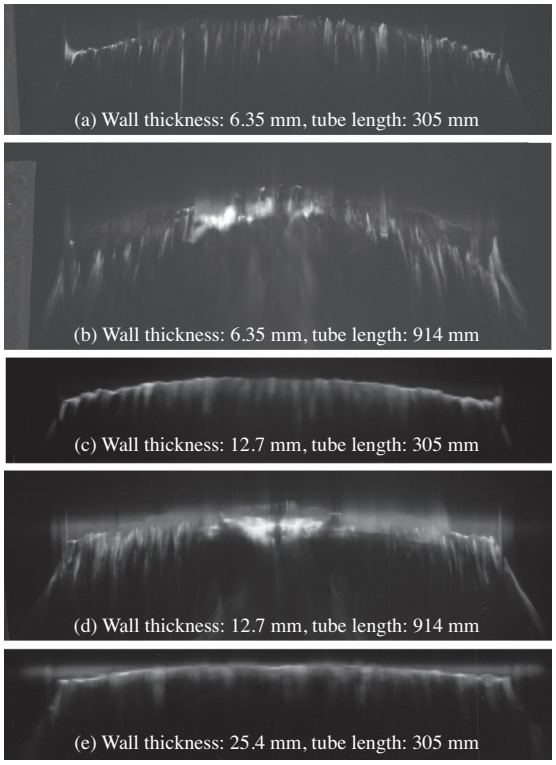

Fig. 8. Streak records. Wave propagation direction is up.

length tubes for each wall thickness tested. This indicates that the wave shape approaches its steady state rapidly (within L/ID = 4). In some cases (b, d, and e in Fig. 8), the streak record shows two waves, with a diffuse or weaker front arriving before the main front. Since the imaging section is PETN paint backed by copper tape, this indicates low-level PETN ignition followed by stronger reaction. This phenomenon, discussed in detail elsewhere,[7] was attributed to precursor window movement separating the inner window surface from the explosive prior to the arrival of the detonation front.

Front quality also suffers due to the small diameter of the tubes used in this study relative to the ANFO prill size. The average prill diameter was approximately 1.7 mm, yielding only about 44 prills across a diameter chord. Front records reflect this discritization of the detonation front. The only way to improve the resolution of the front would be to field larger diameter tubes or smaller diameter ANFO, as has been done for cardboard-confined ANFO.[8–10]

D_n-κ Analysis

DSD analysis is based on the concept that deviations of the normal detonation velocity D_n from the Chapman-Jouguet (CJ) velocity are a function of the curvature κ associated with the local wavefront.[11] In general, the D_n-κ relationship is derived experimentally from detonation velocity and wavefront shape measurements in a rate-stick test. Energy loss from the detonation reaction zone to the confiner wall slows the detonation front near the wall and results in flow divergence and movement of the sonic plane towards the shock. This is manifested by increasing curvature with radius from the rate-stick center to the edge. Varying degrees of curvature can thus be imposed on a detonating explosive rate stick by modifying the confining material.

Calculation of D_n and κ

Experimental front shapes are typically fit to an analytic equation $z(r)$ with a similar characteristic shape. The normal velocity D_n can then be found from

$$D_n = \frac{D}{\sqrt{1+z'}} \tag{1}$$

where $z' = dz/dr$, D is the axial detonation phase velocity obtained from the wall of the rate stick, and r is the radius. Curvature κ can be expressed as

$$\kappa = \frac{z''}{[1+(z')^2]^{3/2}} + \frac{z'}{r\sqrt{1+(z')^2}} \tag{2}$$

with $z'' = d^2z/dr^2$. Use of a C^2 analytic function $z(r)$ yields smooth values of the first and second derivatives $z'(r)$ and $z''(r)$ and avoids errors that would result from direct numerical differentiation of the experimental wave front for the granular explosive used. When using this method, it is critical that the specified fit accurately represent the actual wave shape.

Analytical Wavefront Forms

An equation often used to fit the detonation shape is of the form

$$z_1(r) = -\sum_{i=1}^{n} a_i \ln\left[\cos\left[\eta\frac{\pi}{2}\frac{r}{R}\right]\right]^i \quad (3)$$

where r is the local radius and R is the maximum radius of the charge (37.5 mm). Parameters a_i and η are fitting constants where $0 < \eta < 1$ and n is typically chosen as 1 or 3.[8] However, Eq. 3 does not allow for the non-monotonic variation in curvature present in the outer radii of the wave shapes in Fig. 8.

While exploration of the fitting forms that best represent the aluminum-confined ANFO data is still ongoing, a function can be formulated to match the observed curvature trend. In the present manuscript, we have chosen the Kelvin function $Kei(x)$,

$$z_2(r) = b\,Kei\left[\zeta\left(\frac{r}{R}\right)^m\right] \quad (4)$$

as a possible fitting candidate. More explicitly, this function is the imaginary part of a 0^{th}-order modified Bessel function of the second kind. It is able to accommodate the rapid decrease and possible reversal in curvature observed in the wave-shape data.

Unfortunately, the current implementation of $Kei(x)$ is unable to simultaneously recover the non-zero wavefront curvature for small radii and properly fit the outer radii. Our current solution is to utilize a composite function z_c that smoothly blends Eqs. 3 and 4 together as shown in Fig. 9.

$$z_c(r) = \omega_1\, z_1 + \omega_2\, z_2 \quad (5)$$

The weighting parameters ω_1 and ω_2

$$\omega_{1,2} = \frac{1}{2}\left[1 \pm \cos\left(\pi\frac{r}{R}\right)\right] \quad (6)$$

favor z_1 near $r = 0$ and z_2 near $r = R$.

Fit to the Aluminum-Confined ANFO data

Fitting the composite function to the data of Fig. 8 obtained from the 305-mm-long tubes only yields the wave shapes shown in Fig. 10 and the fitting parameters shown in Tab. 2. While apparent in the streak records, the decrease in overall wavefront curvature due to the increased confiner thickness is much more obvious when the fits are plotted relative to one another.

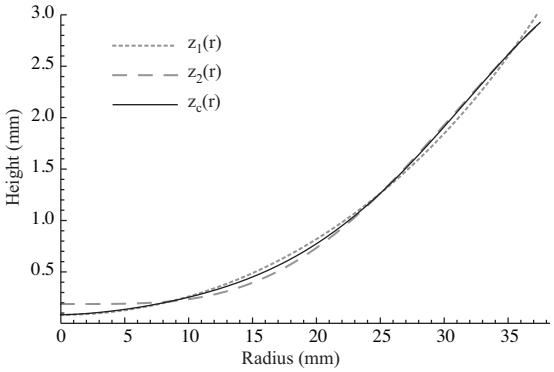

Fig. 9. Wavefront fits for test 12-305.

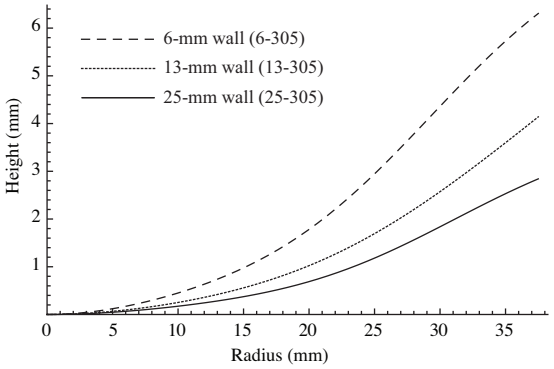

Fig. 10. Front shape variation with confinement.

Application of Eqs. 1 and 2 to each fit then yields D_n and κ as a function of radius. The variation in these parameters across the wavefront is shown in Fig. 11 test 25-305. The normal detonation velocity is highest at the center of the charge and decreases with increasing radius as the normal to the wavefront diverges from the longitudinal tube axis. The normal velocity then increases slightly near the confining wall as the wavefront normal turns back

Table 2. Wavefront fitting parameters.

Test Name	a_1 (mm)	η	b (mm)	ζ	m
6-305	105	0.223	9.54	2.27	2.05
12-305	8.24	0.591	12.5	1.09	1.74
25-305	5.49	0.604	4.58	2.06	2.21

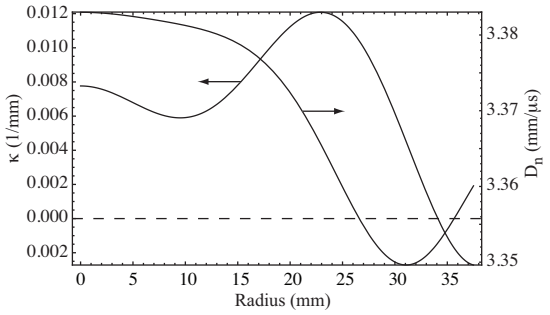

Fig. 11. D_n and κ versus r for test 12-305.

toward the axis. Curvature is seen to start at a positive value that decreases to a local minimum near 10 mm, increases to a global maximum near 23 mm, and then crosses to a negative value near the confining wall.

A plot of D_n as a function of κ for all of the 305-mm-long tests is shown in Fig. 12. The trends

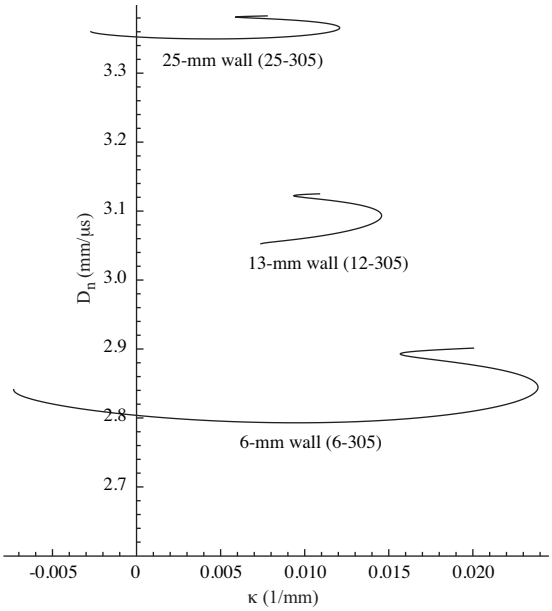

Fig. 12. D_n versus κ versus r for all 305-mm-long tests.

seen in Fig. 11 are evident in all traces and are markedly different from prior ANFO data obtained with light confinement.[8] In particular, each D_n-κ curve exhibits two rollovers that are due to a local minima or maxima in curvature along the radius. The local maximum in κ is apparent in the streak records and demonstrates the effect of the aluminum confinement. However, we believe that the local κ minimum is an artifact of the composite fitting form (particularly the weighting function) and is not present in the experimental data. Ongoing study of the best fitting form will explore this issue.

The Effect of Confinement on the Front Shape

Variations in confinement will obviously affect the curvature of the detonation wavefront. It is instructive to consider the resulting wave shapes for confiners that (a) remove energy from the reaction zone (sink confinement), (b) neither remove nor contribute energy (perfect confinement), and (c) add energy (energetic confiner) to the subsonic region of the reaction zone.

Most confiners for high explosives yield at pressures well below those produced by the detonation shock. For these materials, arrival of the detonation at the HE-confiner interface drives an inert shock into the confiner, causing the HE-confiner interface to move outwards. The outward motion of this interface expands the partially reacted HE materials and removes energy from the flow, inducing wave curvature and resulting a decreased bulk detonation velocity ($D < D_\infty$) as shown in Fig. 13a. For a given detonation, lower impedance confiners are accelerated to higher velocities (up to a limiting maximum), allowing for more interface movement, translating to increased reaction zone energy loss and more wavefront curvature.

A perfect confiner is able to constantly match the flow pressure and velocity along the HE-confiner interface such that no energy is transmitted to or from the reaction zone. The result is that the detonation front shape is perfectly flat (Fig. 13b), as it would be in a charge of infinite radius and the detonation velocity is $D = D_\infty$. In general, the only perfectly matched confiner for a given HE is itself. For gaseous detonations at atmospheric pressures, metal walls also approximate an ideal confiner due to their much higher impedance.

Energetic confiners are actually able to *add* energy at or ahead of the detonation reaction zone near the HE-confiner interface. As shown in Fig. 13c, this energy addition accelerates the detonation near the interface and results in negative curvature rel-

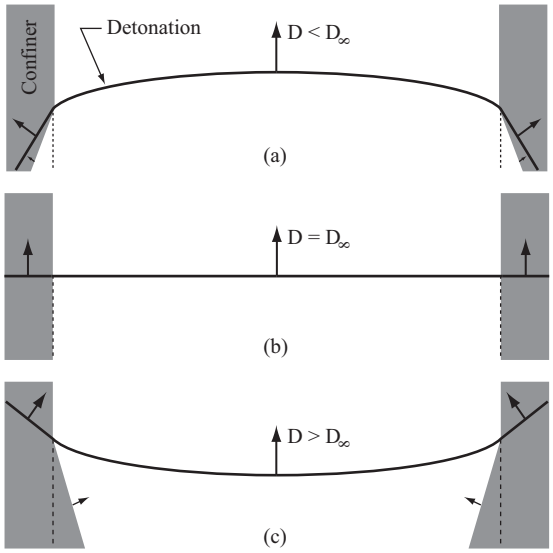

Fig. 13. Wave curvature that would result from (a) sink, (b) perfect, and (c) energetic confinement. Shocked confiners are shown for simplicity.

ative to the case of weak confinement. Unlike the previous two cases, this converging wave configuration is unsteady; for constant energy injection, the wave shape will transition to that of Fig. 13b, with $D > D_\infty$.

The observed front shapes in Fig. 8 appear to be a combination of cases (a) and (c). Positive curvature is obviously present in the central region of the flow, however near the edge of the charge negative curvature appears. It would be presumptuous to assume that the front shapes are a steady-state phenomenon given that negative curvature is unsteady and that the charges tested were short in length. However, the observed waveforms are definitely quasi-steady or, at least, persistent given their presence in both the shorter (L/ID = 4) and longer (L/ID = 12) tubes tested. In a related work, Short et al.[12] numerically explore this problem in further detail.

We also note that the wavefront shapes observed in the current study are markedly different than the results from Belcher and Eden[1] in that their precursor edge effects not only modified the detonation shape near the wall, but spread across the entire wave profile after propagating approximately two charge widths. However, their difference between D and the confiner sound speed was much larger (5.2 mm/μs) than in the present study ($\sim$2.1 mm/μs).

Conclusion

Detonation waves were propagated in aluminum tubes filled with the non-ideal high explosive ANFO. Tube wall thickness varied from 6.35 to 25.4 mm while lengths of 305 and 914 mm were used. This configuration was of interest because the sound speed of the aluminum confiner exceeded the detonation velocity, preventing a shock from forming in the tube wall and allowing the aluminum to transport energy from behind the detonation front to the undisturbed explosive upstream.

Front-shape records showed maximum curvature away from the wall, with different characteristic wave shapes than observed in weakly confined ANFO. Detonation and aluminum stress wave velocities were recorded with shorting, ionization, and piezoelectric pins embedded in the tube wall. In all cases, increasing the tube wall thickness led to higher detonation velocities and less wavefront curvature, as predicted by prior work.[3] The precursor motion of the aluminum tube and window ahead of the detonation front is discussed in a separate study.[7]

Calculation of the D_n-κ relationship for the 305-mm-long tubes tested indicated that prior wavefront fits of the form $\ln[\cos(r)]$ did not properly account for the decrease in curvature near the wall. A new analytical fitting form was proposed. The maxima in wavefront curvature with increasing radius resulted in a rollover on the D_n-κ plot. The proposed fitting form also was found to exhibit a second artificial minima in curvature, which was not present in the experimental data and highlighted the need for further development of a fitting form able to represent the new wave shapes.

The velocity, front-shape, and D_n-κ data presented are essential to understand and accurately model the behavior of low-detonation-velocity explosives in higher-sound-speed confiners. Future tests will further explore the observed phenomena in larger-diameter, longer-length tubes to verify the propagation behavior and obtain higher-fidelity front-shape measurements that are unaffected by the early wall motion.

Acknowledgements

The authors are grateful to Robert Mier, John Morris, and Larry Vaughan for their assistance fielding these experiments and to Matt Briggs, Steve Hare, and Mike Shinas for their expertise with the PDV system. This work was supported by the DOE and managed by Jim Koster and David Robbins.

References

1. G. Eden and R. Belcher, "The effects of inert walls on the velocity of detonation in EDC35," in *Proceedings of the 9th International Symposium on Detonation*, pp. 831–841, Office of Naval Research, 1989.
2. H. Arai, Y. Ogata, Y. Wada, A. Miyake, W. Jung, J. Nakamura, and T. Ogawa, "Detonation behavior of ANFO in resin tubes," *Sci. Technol. Energetic Mat.* **65**, pp. 201–205, 2004.
3. G. Sharpe and J. Bdzil, "Interactions of inert confiners with explosives," *Journal of Engineering Mathematics* **54**, pp. 273–298, 2006.
4. T. Aslam and J. Bdzil, "Numerical and theoretical investigations on detonation confinement sandwich tests," in *Proceedings of the 13th International Symposium on Detonation*, pp. 761–769, Office of Naval Research, 2006.
5. T. Aslam and J. Bdzil, "Numerical and theoretical investigations on detonation-inert confinement interactions," in *Proceedings of the 12th International Symposium on Detonation*, pp. 483–488, Office of Naval Research, 2002.
6. J. Bdzil, T. Aslam, R. Catanach, L. Hill, and M. Short, "DSD front models: Nonideal explosive detonation in ANFO," in *Proceedings of the 12th International Symposium on Detonation*, pp. 409–417, Office of Naval Research, 2002.
7. S. Jackson, C. Kiyanda, and M. Short, "Experimental observations of detonation in Ammonium-Nitrate-Fuel-Oil (ANFO) surrounded by a high-sound-speed, shockless, aluminum confiner," in *Accepted to the Proceedings of the 33rd International Combustion Symposium*, The Combustion Institute, 2010.
8. R. Catanach and L. Hill, "Diameter effect curve and detonation front curvature measurements for ANFO," in *Shock Compression of Condensed Matter*, pp. 906–909, American Institute of Physics, 2001.
9. M. Short, T. Salyer, T. Aslam, C. Kiyanda, J. Morris, and T. Zimmerly, "Detonation shock dynamics calibration for non-ideal HE: ANFO," in *Shock Compression of Condensed Matter*, pp. 189–192, American Institute of Physics, 2006.
10. T. Salyer, M. Short, C. Kiyanda, J. Morris, and T. Zimmerly, "Effect of prill structure on detonation performance of ANFO," in *Accepted to the Proceedings of the 14th International Symposium on Detonation*, Office of Naval Research, 2010.
11. J. Bdzil and T. Aslam, "Detonation front models: Theories and methods," Tech. Rep. LA-UR-02-942, Los Alamos National Laboratory, Los Alamos, NM, 2002.
12. M. Short, J. Quirk, C. Kiyanda, S. Jackson, M. Briggs, and M. Shinas, "Simulation of detonation of Ammonium Nitrate Fuel Oil Mixture Confined by Aluminum: Edge angles for DSD," in *Proceedings of the 14th International Symposium on Detonation*, Office of Naval Research, 2010.

Discussion

Matei Radulescu, U. of Ottawa

Your x-t diagram of the detonation position and elastic wave in the confiner show an in-plane sequence of acceleration and deceleration. What are these due to?

Reply by S. Jackson

We currently are unable to provide a definitive explanation for this phenomenon. It could simply be an initiation transient. Alternatively, the oscillations may be due to a coupled interaction between the confiner and the detonation, which is not predicted to reach steady-state, but rather a quasi-steady propagation condition. [12]